Low-lying resonances in electron-argon scattering: Measurements at 5-meV resolution and comparison with theory

K. Franz,[1] T. H. Hoffmann,[1] J. Bömmels,[1] A. Gopalan,[1] G. Sauter,[2] W. Meyer,[2] M. Allan,[3] M.-W. Ruf,[1] and H. Hotop[1]
[1]*Fachbereich Physik, Technische Universität Kaiserslautern, D 67653 Kaiserslautern, Germany*
[2]*Fachbereich Chemie, Technische Universität Kaiserslautern, D 67653 Kaiserslautern, Germany*
[3]*Département de chimie, Université de Fribourg, CH 1700 Fribourg, Switzerland*
(Received 13 May 2008; published 28 July 2008)

Combining a laser photoelectron source with a triply differentially pumped supersonic beam target and several electron multipliers for simultaneous detection of electrons elastically scattered into the angles 22.5°, 45°, 90°, 112.5°, and 135° and of metastable atoms due to inelastic scattering, we have carried out an improved study of electron-argon scattering over the energy range 11.0–13.7 eV with experimental energy widths around 5 meV. In addition, the Fribourg scattering apparatus has been used for careful remeasurements of the differential cross section and the resonance structure in the energy range of the two lowest anion resonances over the full angular range at a resolution of about 13 meV. Accurate values for the energies, the widths (2.3 ± 0.2 meV), and the fine-structure separation (172.7 ± 0.2 meV) of the low-lying $Ar^-(3p^5 4s^2\ ^2P_{3/2,1/2})$ Feshbach resonances have been determined from the two experiments by detailed partial-wave analyses of the resonance profiles using several sets of energy-dependent background phase shifts; these include an accurate set obtained with a coupled-cluster calculation involving a soft box potential. Moreover, the excitation function for the production of metastable $Ar^*(3p^5 4s\ ^3P_{2,0})$ atoms has been measured from threshold to 13.7 eV. From a fit to its onset, the absolute electron energy scale is established to within ± 0.3 meV; in addition, the energies and widths of some higher-lying resonances (12.9–13.5 eV) have been determined and are compared with the results of earlier experiments and of a recent *B*-spline *R*-matrix calculation. In connection with calibration experiments involving He atoms, we carried out an improved measurement of the $He^-(1s2s^2\ ^2S_{1/2})$ resonance and deduced a natural width of 10.9 ± 0.3 meV.

DOI: 10.1103/PhysRevA.78.012712 PACS number(s): 34.80.Bm, 34.80.Dp, 31.15.vj, 32.70.Jz

I. INTRODUCTION

Collisions of low-energy electrons with atoms, molecules, and ions are important elementary processes in technical and natural plasmas including gaseous discharges, flames, laser plasmas, high-current switches, arcs, and stellar atmospheres. These processes have been investigated for a long time, but most notably since the 1960s with the availability of improved vacuum and detector technologies and following the discovery of narrow resonances in electron scattering from atoms and molecules [1–9]. Using conventional equipment for electron-energy selection (e.g., spherical or cylindrical electrostatic condensers), typical energy widths in low-energy electron scattering experiments involving gaseous targets have been in the range 20–60 meV full width at half maximum (FWHM). In a few cases, energy widths down to about 7 meV (FWHM) have been obtained [9–14].

As a promising alternative to reach very high resolution, near-threshold photoionization of atoms has been exploited as a source for monoenergetic electrons. This approach has been applied in several experiments to study anion formation due to low-energy electron attachment [9,15] as well as total [16–19] and angle-differential [16,17,20–23] electron scattering cross sections. In a pioneering elastic scattering experiment involving He, Ar, and N_2, Gallagher and coworkers achieved an effective energy resolution of 5–6 meV [20,21]. More recently, Gopalan *et al.* [22] combined a laser photoelectron source with a triply differentially pumped supersonic beam. In a first application they restudied the $He^-(1s2s^2)$ resonance at a resolution of 7.5 meV. In subsequent work on the narrow $Ne^-(2p^5 3s^2\ ^2P_{3/2,1/2})$ Feshbach resonances, energy widths down to 4 meV were achieved at satisfactory signal-to-background ratio [23], thus yielding accurate values for the resonance widths and resonance energies. The latter were referenced to the onset for the production of the lowest metastable level $Ne^*(3s\ ^3P_2)$, which was measured simultaneously with the elastic scattering.

In the present paper, we describe an improved study of resonance structure in electron-argon scattering over the energy range 11–13.7 eV at experimental energy widths around 5 meV with simultaneous detection of the elastically scattered electrons at five scattering angles from 22.5° to 135°. In addition, the Fribourg scattering apparatus has been used for careful remeasurements of the differential cross section (DCS) in the energy range of the two lowest anion resonances over the full angular range at a resolution of 13 meV. Previous high-resolution work on Ar until 1993 was summarized by Buckman and Clark [5]. Subsequently, Dubé *et al.* [24] as well as Hammond [25] reported energies and widths of the low-lying $Ar^-(3p^5 4s^2\ ^2P_{J=3/2,1/2})$ Feshbach resonances with reduced error bars, as deduced from detailed analyses of the experimental data measured with resolutions of about 30 meV [24] and 12 meV [25], respectively. While the resonance width 2.3(2) meV (i.e., 2.3 ± 0.2 meV), determined by Dubé *et al.* [24], confirmed the value 2.5(5) meV, recommended by Buckman and Clark [5], the resonance widths 3.4(2) meV and 3.2(2) meV for $J=3/2$ and $J=1/2$, obtained by Hammond [25], are distinctly higher, also in comparison to the recent theoretical values 2.2 and 2.1 meV, predicted by Zatsarinny and Bartschat [26] from *B*-spline *R*-matrix calculations.

The present resonance spectra were evaluated with detailed partial wave analyses involving several sets of energy-dependent background phase shifts, and the energy scale was calibrated with sub-meV precision with reference to the onset for the production of metastable $Ar^*(4s\ ^3P_2)$ atoms. Our recommended value for the resonance width of 2.3(2) meV confirms the earlier experimental results [5,24] and also agrees with the *B*-spline *R*-matrix values quoted above. Our resonance energies are in excellent agreement with those of Hammond [25].

Using an additional electron multiplier at the appropriate position, we also measured the excitation function for the production of metastable $Ar^*(3p^5 4s\ ^3P_{2,0})$ atoms from threshold to 13.7 eV. In particular, we determined the energies and widths of some higher-lying resonances in the range 12.9–13.5 eV and compare them with previous experimental [5,27,28] and theoretical results [26].

The paper is organized as follows. In Sec. II we summarize the theoretical formulas used for the analysis of the elastic scattering resonance data. In Sec. III we describe the experimental apparatus in Kaiserslautern and some test measurements mainly related to cluster formation in the supersonic argon target beam. We briefly dwell on the Fribourg experiment which uses an effusive target beam. In Sec. IV we report the experimental results and the analyses of the resonance profiles; moreover, we present a comparison with theoretical results. We conclude with a brief summary.

II. THEORETICAL DESCRIPTION

Partial wave analysis of the angle-dependent $Ar^-(3p^5 4s^2\ ^2P_{3/2,1/2})$ resonance profiles

The DCS $d\sigma/d\Omega$ for elastic potential electron scattering in the presence of significant spin-orbit coupling is given by [23,29]

$$d\sigma/d\Omega(\theta,E) = |f(\theta,E)|^2 + |g(\theta,E)|^2, \tag{1}$$

where the direct and exchange amplitudes f and g are given by partial wave sums as follows:

$$f(\theta,E) = (2ik)^{-1}\sum_{L=0}^{\infty} ((L+1)\{\exp[2i\delta_L^+(E)] - 1\} + L[\exp[2i\delta_L^-(E)] - 1\ \})P_L(\cos\theta), \tag{2}$$

$$g(\theta,E) = (2ik)^{-1}\sum_{L=0}^{\infty} \{\exp[2i\delta_L^+(E)] - \exp[2i\delta_L^-(E)]\}P_L^1(\cos\theta). \tag{3}$$

Here, k is the wave vector of the electron and the functions $P_L(\cos\theta)$ are the standard Legendre polynomials while $P_L^1(\cos\theta)$ $(L \geqslant 1)$ denotes an associated Legendre polynomial. Furthermore, δ_L^+ and δ_L^- represent the phase shifts in the partial waves with orbital angular momentum $L \geqslant 1$ and total electronic angular momenta $J^+ = L + \frac{1}{2}$ and $J^- = L - \frac{1}{2}$, respectively. In the absence of spin-orbit interaction, $\delta_L^+ = \delta_L^- \equiv \delta_L$ and $g(\theta,E) = 0$. In the energy range of the spin-orbit split $Ar^-(3p^5 4s^2\ ^2P_{3/2,1/2})$ Feshbach resonances (with an energy separation close to that of the $3p^5$ core—i.e., close to 0.18 eV) the phases δ_L^+ and δ_L^- for the partial wave $L=1$ attain significantly different values due to the additional contribution of the respective resonance phases δ_r^+ and δ_r^-; they are given by the expression [29]

$$\delta_r^{\pm} = -\,\mathrm{arccot}[2(E - E_r^{\pm})/\Gamma^{\pm}], \tag{4}$$

where the plus and minus sign denote the $^2P_{3/2}$ and $^2P_{1/2}$ resonance, respectively. The resonant phase shifts $\delta_r^{\pm}(E)$ rise from 0 to π when the electron energies increase from lower to higher values through the respective resonance energy $E_r^{\pm}$; the breadth of the resonance region is characterized by the resonance width $\Gamma^{\pm}$.

For elastic electron scattering from argon atoms at energies around the $Ar^-(4s^2\ ^2P_{3/2,1/2})$ resonances [5], partial waves higher than $L_c = 3$ do not penetrate significantly to the inner part of the atom (see, e.g., [30,31]) and hence predominantly sample the long-range part of the electron-atom interaction, dominated by the dipole polarization potential $V_{pol} = -\alpha(2r^4)^{-1}$ [α is the atomic polarizability, $\alpha(\mathrm{Ar}) = 11.075 a_0^3$ [32], a_0 is the Bohr radius]. For $L > L_c = 3$, the phases δ_L^+ and δ_L^- are very similar. As shown by Thompson [33], the contribution to the scattering amplitude due to partial waves $L > L_c$ is well represented by the expression

$$f_B(L > L_c) = (\pi\alpha k/a_0)[(1/3) - (1/2)\sin(\theta/2) - \sum_{n=1}^{Lc}[(2n+3)(2n-1)]^{-1}P_n(\cos\theta). \tag{5}$$

Using Eqs. (1)–(5) and appropriate (energy-*dependent*) background phase shifts (see Secs. III D and IV B), DCSs were calculated and convoluted with a Gaussian function of width ΔE in order to simulate the energy resolution function of the experiment. Finally, they were fitted to the measured resonance profiles, using $\Gamma^{\pm}$, $E_r^{\pm}$, and ΔE as adjustable parameters.

III. EXPERIMENT AND DATA ANALYSIS

Results from two different experimental setups in Kaiserslautern [22,23] and Fribourg [13,14] will be reported. We focus on recent improvements and on test measurements relevant for the target argon.

A. Experimental setup in Kaiserslautern

The apparatus combines a laser photoelectron source with a collimated supersonic beam target (diameter 4.3 mm in the scattering region, beam to background gas density >100) [34], yielding a low *a priori* energy spread in the electron beam and negligible Doppler broadening, respectively.

The vacuum system consists of several separately pumped chambers. The nozzle chamber, the intermediate chamber, and the dump chamber create the Campargue-type [35] supersonic beam; test measurements on the influence of argon clusters will be described in Sec. III B. The base (background) pressure in the main chamber, located between the intermediate and the dump chamber, was around 5

$\times 10^{-8}$ mbar (2×10^{-7} mbar) when the target beam was off (on, stagnation pressure $p_0=1$ bar).

The photoelectron production is based on resonant two-step photoionization of potassium atoms in a well-collimated beam (diameter 2 mm, atomic density around 10^8 cm^{-3}) [9,22,36–38]. The potassium beam is generated in a differentially-pumped two-stage oven, operated in the effusive regime [22]. Both hyperfine components of ground state ^{39}K $(4s, F=1,2)$ atoms in the collimated beam are transversely excited to the ^{39}K* $(4p_{3/2}, F=2,3)$ states by the first sidebands of the electro-optically modulated (frequency 220.35 MHz) output of a single-mode cw titanium:sapphire laser ($\lambda_1=766.7$ nm); the latter is long-term stabilized to the atomic transition by crossover saturation spectroscopy in an auxiliary potassium vapor cell [39]. Part of the excited state population is photoionized by interaction with the focused intracavity field of a multimode tunable dye laser (energy width about 0.08 meV, power up to 7 W), operated in the blue spectral region (dye Stilbene 3). The laser diameter is about 120 μm in the 2 mm long photoionization region. Electrons are created very close to threshold ($\lambda_2=455.3$ nm, nominal electron energy below 0.1 meV) in a nearly homogeneous extraction field of typically 10 V m^{-1}. As confirmed by test measurements, the quoted extraction field leads to an associated energy width around 1 meV, in agreement with the width expected from the (calculated) laser diameter. The infrared laser (typical power around 80 mW) is superimposed collinearly with the ionization laser, entering through the terminating mirror [transmission 0.94(1)% at 455 nm and about 98% at 767 nm] of the blue laser. The infrared laser is thus also brought to a spherical focus with a diameter somewhat wider than that of the ionization laser. The photoelectron current was independent of the infrared laser power at levels above 10 mW, and typical photoelectron currents were in the range 50–90 pA. At these currents the energy broadening due to the photo-ion space charge is expected to be below 2 meV [23,38].

Following the primary acceleration in the photoionization chamber, the electrons are brought to the energy of interest by an electron optical system which directs the nearly parallel electron beam (width and height about 2 mm and 1 mm, respectively) onto the perpendicular target beam. Electron optical and geometrical considerations (including the divergence of the target beam, half angle 0.015 rad) indicate that the deviations from perpendicular impact are at most ± 0.03 rad, leading to negligible Doppler-type energy broadening [22,23]. The electron beam is dumped in a Faraday cup (Fig. 1) which consists of an outer shield S (at ground potential), a cylindrical outer collector OC (typically at +12 V), and an inner collector IC (typically at +38 V, thus sampling nearly the complete electron flux).

The target beam is surrounded by the reaction chamber (Fig. 1) which consists of a cylinder (diameter 50 mm), made of four segments (positioned around the angles 0°, 90°, 180°, and 270°). Different potentials may be applied to these electrodes, thus allowing for possible compensation of residual electrostatic fields in the reaction volume along and perpendicular to the electron beam direction in the horizontal plane. Field compensation in the vertical direction (out of the plane in Fig. 1) can be achieved as well by applying appropriate potentials to the entrance and exit plate, terminating the reaction chamber in the nozzle beam direction. The walls are coated with colloidal graphite (Kontakt Chemie, Graphit 33) to obtain (nearly) homogeneous surface potentials. Since test measurements showed no significant improvement of the energy resolution when additional fields were applied in the three possible directions, the electrodes of the reaction chamber were all kept at ground potential. Magnetic fields were shielded with a double layer of mu metal (each 1.5 mm thick), which reduces the residual dc magnetic field components in the main chamber to values below 0.1 μT in the horizontal plane and well below 0.6 μT in the vertical direction.

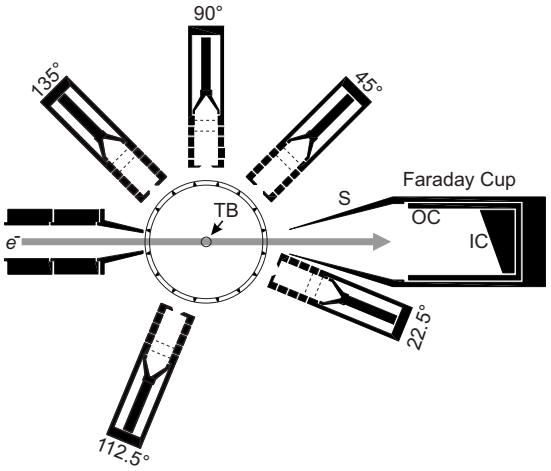

FIG. 1. Horizontal cut through reaction chamber and detectors.

Five electron detectors, each equipped with a retarding electric field and a channel electron multiplier (Sjuts Mod. KBL 10 RS, diameter of entrance cone 10 mm), serve to measure simultaneously the intensity of elastically scattered electrons at the fixed scattering angles $\theta=22.5°$, 45°, 90°, 112.5°, and 135° (see Fig. 1). A rectangular entrance aperture (4 mm wide, 6 mm high, located 32.5 mm from the scattering center) limits the angular acceptance range of the electron detectors to $\pm 3.5°$. It is followed by a circular lens element (diameter 10.6 mm, length 4 mm) and a pair of grids (diameter 10.6 mm) which form the retarding field, rejecting inelastically scattered electrons. Because of the well-defined scattering region, electrons from all volume elements of the scattering region are expected to view the detectors with equal detection solid angles. In some cases, the relative overall detection efficiencies of the five detectors were determined *in situ* by measuring the elastic scattering signals from a helium beam and comparing them with angle-differential cross sections, calculated with accurately known phase shifts for the He atom [40].

An additional electron multiplier (Sjuts, Mod. KBL 20 RS, diameter of entrance cone 20 mm) serves for the detection of long-lived excited ("metastable") Ar*$(3p^5 4s\ ^3P_2, ^3P_0)$ atoms due to inelastic electron scattering. It is mounted at an angle of 4.8° off the mean target beam direction (out of the plane of Fig. 1) and samples an angular range of $\pm 2.8°$. Its position is appropriate for the detection of metastable Ne*

atoms [23]. For optimal sampling of metastable Ar* atoms it would have to be mounted closer to the target beam axis, but this would raise the background gas pressure and also lead to a substantial gas flow into the channel multiplier. Therefore, we left the metastable atom detector in the position optimal for Ne* detection. Ground state argon atoms (flow velocity $u=[5k_BT_0/(2\ m_{Ar})]^{1/2}=560$ m/s at $T_0=300$ K), which are excited to the metastable Ar*$(4s\ ^3P_2)$ level by a perpendicular monoenergetic electron beam at threshold [transition energy $E(^3P_2)=11.548\ 354(7)$ eV, obtained from spectroscopic data in [41,42] with the conversion 806 554.445(69) m^{-1}/eV [43]], are deflected by a (lab) angle of 2.84°. At an electron energy of 1.2 eV above threshold, for example, the deflection angles are spread over the range 2.1°–3.9°. The detection of metastable Ar*$(4s\ ^3P_2)$ atoms serves an important purpose: based on the well-known threshold energy and the theoretical cross section for the production of Ar*$(4s\ ^3P_2)$ atoms (see below), one can precisely determine—by comparing the measured yield for metastable atom production with that obtained by convolution of the theoretical cross section with an appropriate resolution function—both the absolute electron energy scale *and* the effective energy width of the scattering experiment (see [22,23] for more details on the kinematics).

The electron energy width is limited by the potential drop of the accelerating field across the photoionization volume (about 1 meV) by the effects associated with photo-ion space charge (below 2 meV; see above) and by drifts and ac fluctuations of the potential difference between the photoionization volume and the reaction region. Custom-made voltage supplies, based on 16-bit high precision digital-to-analog converters (accuracy better than 152 μV over the full voltage range), have been built as well as a versatile graphical data acquisition system [22]. The linearity of the voltage scale has been verified by measuring the output voltage with a precise multimeter (Keithley 2700, stated resolution 10 μV, accuracy 30 ppm). Thorough design of the electronic circuits, careful cabling (avoiding ground and shield loops) and filtering by ferrite cores ensure low noise and ripple figures in the mV range. In view of the proliferation of communication using radio-frequency waves, electromagnetic interference may influence the energy resolution; electromagnetic field measurements in the laboratory did not yield conclusive evidence. So far, the narrowest observed energy resolution amounted to 4 meV [23], somewhat above the expectation, but still the best achieved in electron scattering experiments in the gas phase (we note that in laser photoelectron attachment experiments sub-meV resolution has been demonstrated [44,45], but in these experiments the electrons reacted in the same volume where they were created). In the present argon experiments, energy widths down to 4.5 meV were achieved.

A critical point are (differential) drifts in the surface potentials of the electrodes surrounding the electron source and the scattering region. These drifts influence the effective energy $E=eU_{SP}$ of the incident electrons through variations of the effective potential difference U_{SP} between the scattering region and the photoelectron source volume. The voltage U_{SP} is the sum of the average 'contact' potential difference $U_{SP,C}\equiv\Phi_S-\Phi_P$ between these two volumes and the potential difference $U_{SP,EX}$ supplied by the external voltage used to control the electron energy. Variations of $U_{SP,C}$ and thus U_{SP} are diagnosed by measuring the variation of the energy position of a sharp feature in the electron scattering cross section [here of the $Ar^-(3p^54s^2\ ^2P_{3/2})$ resonance] with time. The voltage $U_{SP,C}$ is observed to be negative due to the fact that the surfaces in the photoelectron production chamber have a higher coverage with potassium than those in the scattering chamber. A potassium layer on the graphite coating generally leads to a shift in the surface potential to positive values. The long-time variation of the voltage $U_{SP,C}$ normally exhibits a rather smooth trend with typical slopes of $\Delta U_{SP,C}/\Delta t\approx -(1-3)$ meV/h. Venting of the main chamber leads to opposite, steplike variations of $U_{SP,C}$ [23].

B. Test measurements with the Kaiserslautern apparatus

1. Response of the electron detectors

In the present investigations—in contrast to the previous work on He [22] and Ne [23]—we faced some problems with the data analysis related to the presence of argon clusters in the supersonic target beam (see below). In this connection, we took a closer look at the response of the five detectors and, for some sets of measurements, carried out an *in situ* detector calibration by measuring the elastic scattering signals from a He beam. Note that for a nozzle at room temperature, the He supersonic beam (and likewise the Ne beam) does not contain clusters in contrast to Ar (see below and [34]). Thus, for He (and Ne) the detector signals for elastic scattering reflect the atomic density in the scattering volume, and they are directly proportional to the respective atomic angle-differential cross sections. For He, these elastic cross sections are known at the 1% level of accuracy at energies up to about 19 eV from the phase shifts calculated by Nesbet [40].

In Fig. 2 we show retarding potential curves of the scattered electron intensities, measured with the five detectors at an incident electron energy $E=11$ eV for a supersonic He beam target (left panels: stagnation pressure $p_0=5$ bar, nozzle temperature $T_0=300$ K) and for a supersonic Ar beam target (right panels: $p_0=1$ bar, $T_0=300$ K). The curves were obtained by varying the voltage $U_{G,EX}$ applied to the retarding grid in front of the channel electron multiplier; the grid voltage is given with reference to the lower potential of the voltage source defining $U_{SP,EX}$. If the contact potential difference $U_{GP,C}\equiv\Phi_G-\Phi_P$ between the detector grid and the photoelectron source volume were zero, the steplike increase of the elastically scattered electron signal would occur at an applied grid potential $U_{G,EX}=0$ V. The observed steps are shifted to positive grid voltages $U_{G,EX}$ (albeit by different amounts); i.e., the contact potentials Φ_G of all five retarding grids are negative relative to that of the photoelectron source volume Φ_P by an amount specific for each of these grids.

Three sets of data are shown in each diagram: (i) the open circles represent the intensities measured with the target beam on; (ii) the open triangle intensities were obtained with the target beam off, but with diffuse gas admitted to the main chamber at the same (background) pressure as observed with the supersonic beam on. The solid curve represents the dif-

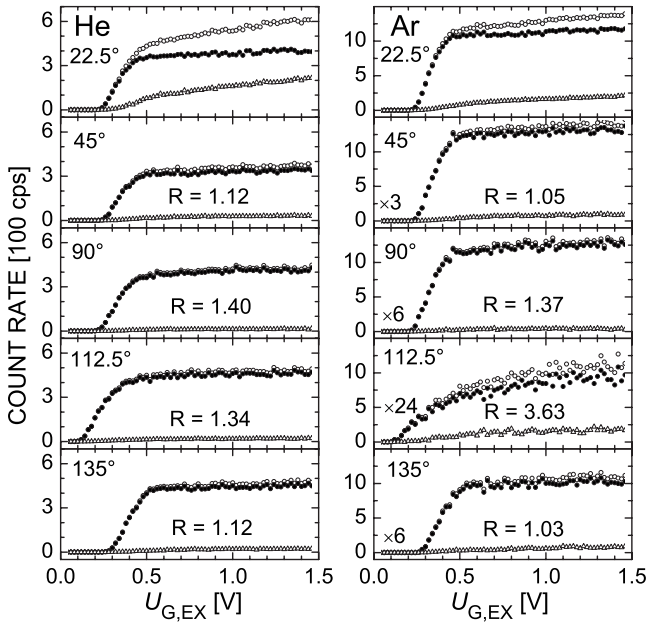

FIG. 2. Retarding potential curves for the scattered electron intensity at an incident electron energy of $E=11.0$ eV: left panels, He; right panels, Ar.

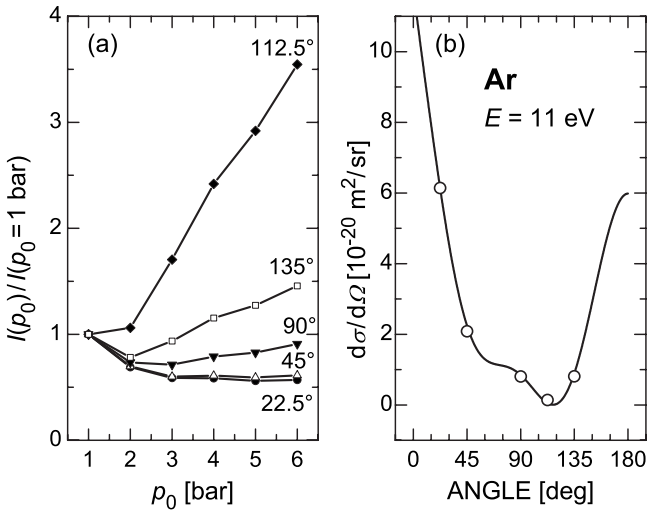

FIG. 3. (a) Dependence of elastically scattered electron intensity on Ar stagnation pressure p_0 at the five detection angles. (b) Angular dependence of the calculated elastic electron scattering cross section [46] (solid curve) at $E=11.0$ eV and measured intensities for $p_0=1$ bar (open circles), normalized to the theoretical cross section at 22.5°.

ference between the intensities (i) and (ii). Following the initial rise from zero intensity, the difference signals all show a plateau (essentially constant intensity) at grid voltages above about 0.6 V. Such a step-plateau-like behavior is expected when only elastically scattered electrons are present.

At forward scattering angles (most notably for He at $\theta=22.5°$), a rather substantial signal is observed when the target beam is off. Since the He density in the scattering region is at least 100 times higher for the supersonic beam target than for the diffuse target, the signal from the latter target (even when an increased path length is considered) appears unexpectedly high. In order to characterize the origin of this "background" signal in more detail, we also carried out measurements with the diffuse gas turned off and found that a substantial or even the dominant part of this background signal had to be attributed to scattering from surfaces. Note that even very low fractions of "halo" electrons in the incident beam (i.e., electrons with trajectories far from the electron beam axis) can lead to significant contributions to the detected signal since they have a high chance to interact with a collimating aperture. We mention that after completion of the work on He [22] and Ne [23] we took several measures to reduce unwanted background: we increased the diameter of the hole in the exit lens of the electron optics from 5 mm [22,23] to 8 mm, and we introduced regularly spaced holes with 8 mm diameter in the cylindrical segments surrounding the scattering volume (see Fig. 1). Moreover, we used an improved Faraday cup, as shown in Fig. 1.

By comparing the angle-dependent, background corrected intensities (evaluated as integrals over the solid curves in Fig. 2 across the range $U_{G,EX}=0.7-1.1$ V) with theoretically predicted DCSs for He [40] and for Ar (e.g., [46]), we obtained the relative responses R of the five electron detectors, as listed in Fig. 2 (the response of the 22.5° detector was set to unity for both He and Ar). From the He data, one concludes that the response of the five detectors differs by no more than 40%. This result is confirmed for Ar with the exception of the detector located at 112.5° for which the response has (seemingly) increased by almost a factor of 3 (relative to the He data). Note that the DCS for Ar atoms has a deep minimum close to $\theta=117°$ (see Fig. 3). Thus, even a rather small amount of target impurity (such as Ar clusters; see below) may lead to seemingly high scattering signals at the $\theta=112.5°$ detector and thus simulate a high response R.

2. Contributions to the electron scattering signals from Ar clusters

It was known from analyses of the argon target density as a function of stagnation pressure p_0 [34] that the formation of Ar clusters becomes significant at pressures p_0 above 1 bar. Measurements of the scattered electron intensity over the range $p_0=1-6$ bars yielded the results shown in Fig. 3(a) where we plot for each detector the pressure-dependent signal, as normalized to the signal observed at $p_0=1$ bar. At the forward angle $\theta=22.5°$ (at which the atomic scattering cross section is the highest for the five selected angles) the normalized signal substantially *decreases* when the pressure is raised from 1 bar to 3 bars, and it stays nearly constant at higher pressures. Almost the same behavior is observed for the 45° detector. At $\theta=112.5$, on the contrary, the signal strongly increases. The dependence observed at $\theta=90°$ and 135° is intermediate between those for 22.5° and 112.5°. These different findings have their origin in the pressure-dependent signal contributions due to atomic and cluster-induced electron scattering. In Fig. 3(b) we show the DCS for Ar atoms at $E=11$ eV (calculated with the theoretical scattering phase shifts reported in [46] which will prove to be realistic; see below) to illustrate the deep cross-section

minimum around 117° (0.0056×10^{-20} m^2 sr^{-1}). For comparison we show the scattered electron signals at $p_0=1$ bar (open circles), as taken from Fig. 2(b) and corrected for the detector response determined with He.

The drop of the 22.5° signal with rising pressure in Fig. 3(a) reflects the fact that the atomic density decreases in favor of cluster formation and as a result of scattering losses between nozzle and skimmer [34]. The rise of the 112.5° signal indicates a strong cluster-induced contribution. At 112.5°, the atomic cross section is so small (and the cluster cross section presumably much higher) that already a low cluster fraction leads to a significant contribution to the scattering signal, while at 22.5° the cluster contribution is relatively small. With the phase shifts of Fon *et al.* [46], the ratio of the atomic DCSs at 112.5° and 22.5° is predicted to be 0.0085; the (response corrected) intensity ratio measured for these two angles at 1 bar, in contrast, amounts to 0.024, indicating a substantial cluster contribution to the scattering signal. Further reduction of the stagnation pressure would have meant severe signal losses, and as a compromise, we kept the stagnation pressure at $p_0=1$ bar throughout the argon measurements. In order to simulate the presence of clusters, we introduced an energy-independent signal contribution in some fit calculations of the resonance structure observed at $\theta=112.5°$ (see Sec. IV).

Interestingly, the shape of the retarding curve in Fig. 2, observed for Ar at 112.5° ($p_0=1$ bar), differs significantly from those seen at the other four angles. We attribute this difference to the fact that electron scattering from Ar clusters produces a significant broadening of the onset due to vibrational excitation of the clusters. It appears tempting to study electron scattering from rare gas clusters at angles for which the atomic DCS exhibits a deep minimum over a certain energy range.

C. Experiment in Fribourg

The measurements at Fribourg were performed using a spectrometer [13,14] with double-hemispherical analyzers, equipped with a magnetic angle changer [47]. The energy resolution was about 19 meV in the energy-loss mode, corresponding to about 13 meV in the incident electron beam, at a beam current of around 400 pA. The energy of the incident beam was calibrated on the 19.365 eV [22] ^2S resonance in helium and is accurate to within ±10 meV. The instrumental response function was determined on elastic scattering in helium, and all spectra were corrected as described earlier [48], with respect to both varying energy and varying angle. Absolute values of the cross sections were determined by the relative flow technique using the theoretical helium elastic cross sections of Nesbet [40] as a reference. The absolute values are accurate to about ±15% (two standard deviations).

IV. RESULTS AND DISCUSSION

A. Choice of the nonresonant electron scattering phase shifts for Ar

For an accurate determination of the resonance parameters via the partial wave analysis outlined in Sec. II, the phase shifts due to nonresonant elastic electron scattering have to be known. These phase shifts do not only determine the absolute values and angular shapes of the nonresonant ("background") cross sections, they also affect the size and shape of the resonance structures via interference with the $L=1$ resonance phase shifts, Eqs. (1)–(4). Phase shifts for electron-Ar scattering in the energy range around 10 eV have been reported in numerous papers, as obtained from semiempirical and *ab initio* calculations [30,46,49–64] and from phase analyses of scattering experiments [24,65–71]. A summary of nonresonant phase shifts, interpolated for the scattering energy $E=11.18$ eV [i.e., midway between the two $Ar^-(4s^2\,^2P_{3/2,1/2})$ resonances], gave the following average values and confidence intervals for the partial waves $L=0$–3: −1.23(±5%), −0.61(±10%), 1.0(±10%), and 0.11(±15%) rad, respectively [72]. Note the unusually large value of the d-wave phase shift. It indicates a broad shape resonance around 7 eV which is due to deep penetration of the $3s^23p^6$ shell by d electrons which are not subject to orthogonality constraints. (This resonance narrows for the subsequent atoms K and Ca and then collapses to an occupied d orbital [73].) The phase shift for d-wave electrons is therefore expected to be sensitive to details of the treatment of the electron-atom interactions at close distances. The scatter of the data is unexpectedly large for a well-studied rare-gas atom. Even for recent measurements, errors between 5% and 10% are quoted for differential cross sections above 5 eV [71]. Since the data are usually restricted to the angular range between 30° and 120°, their inversion to phase shifts may well enhance the uncertainties even if the inversion has been "regularized" by reference to a set of theoretical phase shifts—e.g., [71]. Above 1 eV the phase shifts are generally derived separately for each energy and may show irregularities as functions of energy, preventing reliable interpolation and extrapolation (e.g., the p-wave phase shift of [71] at 10 eV appears to be off by 20%).

Theoretical treatments of electron scattering on atomic or molecular targets still suffer from the notorious difficulties to combine target calculations which provide proper account of electron correlation with an adequate treatment of the continuum electron. For rare-gas atoms, next to direct and exchange interaction with an self-consistent-field-type (SCF-type) target (in mean-field description) the polarization interaction is most crucial. Its treatment has followed three different lines.

Fon *et al.* [46] used the R-matrix method with the argon ground-state Hartree-Fock wave function coupled to a ^1P pseudostate optimized for the ground-state dipole polarizability. The actual polarizability turned out too large by 15%, and deficiencies observed for results below 5 eV were traced to that. Bell *et al.* [55] applied the same approach to the energy region of the Ramsauer-Townsend minimum and found a disturbing sensitivity to the energetic position of a (bound) pseudostate of the compound system $Ar+e^-$, introduced by the pseudo-orbital $4s$. This position was then adjusted to provide the desired minimum location and scattering length, but at the cost of rather low phase shifts for energies around 10 eV.

The polarized orbital (PO) method—a one-electron close-coupling calculation involving the SCF potential of a frozen

target and effective long-range polarization potentials—has been applied at increasing levels of sophistication. The exchange-adiabatic approximation, based on a numerically derived dipole polarization potential [53], produced too small (*s*-wave) phase shifts below 1 eV and rather large (*d*-wave) phase shifts above 5 eV. Both deficiencies could be considerably moderated by inclusion of exchange-perturbation terms [56], dynamic distortion effects [74], polarization terms, and extension to a converged set of higher-order polarizabilities [62]. Since relativistic effects had been shown to be significant for Ar at energies below 1 eV [59], McEachran and Stauffer [64] used their converged PO potential in a relativistic treatment and reported phase shifts over the energy range 0.01–10 eV (in 2004 these calculations were extended on our request to the range 11.0–11.5 eV, for which we are indebted to the authors). They are in excellent agreement with empirical phase shifts from a modified effective range theory (MERT) analysis for energies below 1 eV and also agree rather well with the recent experimental differential cross sections [71] for 2, 3, and 10 eV, respectively. However, systematic deviations appear for the energies 5 eV and 7.5 eV, indicating *d*-wave phase shifts being too high by 7%–9% in this range. This is likely due to the neglect of intratarget correlation: the penetrating *d* electron excludes an important orbital from the correlation space of the target which results in a repulsive potential.

This effect should be accounted for in the *ab initio* calculations by Saha [61] based on a multiconfiguration self-consistent-field (MCSCF) ansatz for the target ground-state wave function (doubly excited configurations from frozen orbitals) and its polarizing states (singly excited configurations from energy-adapted orbitals). The results were somewhat disappointing since the *s*-wave phase shifts turned out much too high at low energies and the *d*-wave phase shifts too large at any energy by up to 20%. Saha later refined his calculations, and results at several energies up to 10 eV were quoted in Table 2 of Ref. [71]. The phase shifts appear much improved in all respects; this was attributed to the inclusion of higher-order polarization terms [71].

The lack of a clear choice for the nonresonant phase shifts at around 11 eV induced an attempt to derive a hopefully reliable set of phase shifts by applying a different *ab initio* method for low-energy electron-molecule scattering cross sections. This method makes full use of the most advanced *ab initio* methods for molecular bound states and has recently been applied very successfully to a notoriously difficult case, the $^2\Pi_g$ resonance of N_2^-, thereby for the first time providing a converged resonance position [75]. The only routine method known to produce reliable dispersion interactions between molecules (analogous to the polarization potential between scattering electron and target) is the coupled-cluster method with singles, doubles, and (perturbative) triples substitutions [CCSD(T)]. Since it provides only energies, the scattering continuum is discretized by putting the compound system in a wide soft-box potential constructed from Gaussian functions. Phase shifts are derived from the electron energy shifts generated by putting the (small) target in the center of the box, just as they are derived in quantum defect theory. The scattering electron orbitals are easily expanded by the usual Gaussian-type functions and new types of two-electron integrals are avoided. High numerical stability has been demonstrated by comparing results from different box potentials, each of which provides phase shifts for four to five collision energies. Excellent agreement was obtained with the benchmark results of Nesbet [40] for He, proving the viability of the scheme. The Ar phase shifts calculated for $L=0-3$ are also very satisfying. At energies below 1 eV there is close agreement with the calculations of McEachran and Stauffer [64] and the empirical phase shifts from the MERT analysis (as discussed in [64]). At the higher energies covered in Ref. [71] (1–10 eV), the agreement with the measured differential cross sections is regularly within the given error bars. In summary, the new phase shifts are believed to be the most consistent values so far over the full energy range up to 15 eV. As will be discussed in detail in [76], the closest agreement with previous phase shifts is observed with those derived from measured differential cross sections by Bitsch (4–15 eV) [65], on the one hand, and with the theoretical values of Saha (1–10 eV, as quoted in [71]), on the other hand.

For the analyses of our resonance scattering experiment it is very important that the chosen background phase shifts produce the correct DCSs and total cross sections around 11 eV. For comparison, we have selected six sets from the theoretical work discussed above and give their (interpolated) phase shifts at 11 eV and their changes over the energy range 11.00–11.36 eV in Table I. As a sensitive test of the theoretical phase shifts, we compare in Fig. 4(a) the corresponding six sets of calculated DCSs with the *absolute* DCS measured at $E=10$ eV by Gibson *et al.* [71] (open circles, 15°–130°) and by Mielewska *et al.* [77] (open diamonds, 60°–180°). Good agreement between the experiment and most theories is observed in the intermediate range of angles (45–90°; see inset). Larger differences between the various theories emerge at small ($<40°$) and large ($>150°$) angles. Over the range 15°–40°, the experimental data support the theoretical results of Fon *et al.* [46] and Sauter and Meyer (SM) [76]. With reference to their results, the forward and backward scattering cross sections come out somewhat low when using the phases of Bell *et al.* [55] or Dasgupta and Bhatia [56], while the reverse is true when the phase shifts of Sienkiewicz and Baylis [59] or McEachran and Stauffer [64] are used. Closer inspection of the (background) phase shifts and cross sections shows that these trends have mainly to do with differences between the *d*-wave phase shifts (Table I). As to the close agreement between the DCS of Fon *et al.* [46] and SM [76], the significant difference between their *d*-wave phase shifts appears to be compensated for by the differences in the phase shifts for *s* and *p* waves, underlining the correlation between the phase shifts of different orbital angular momentum.

At angles above 130°, all calculated DCSs (with the exception of that due to Bell *et al.* [55] which is too low at small angles) stay substantially above the only set of measured values, obtained by Mielewska *et al.* [77] up to 180° with the magnetic angle-changing method [47]. In view of this unsatisfactory situation, we decided to carry out another measurement of the elastic DCS at $E=11.2$ eV (i.e., midway between the two Feshbach resonances) over the full angular

TABLE I. Phase shifts δ_L (L=0, 1, 2, 3) for electron-Ar scattering at the energy E=11.0 eV and their change $\Delta\delta_L$ over the energy range 11.00–11.36 eV.

Authors [reference]	δ_0 (rad) $\Delta\delta_0$ (rad)	δ_1 (rad) $\Delta\delta_1$ (rad)	δ_2 (rad) $\Delta\delta_2$ (rad)	δ_3 (rad) $\Delta\delta_3$ (rad)
Bell *et al.* [55][a]	−1.2508	−0.6526	+0.7289	+0.1070
	−0.0222	−0.0154	+0.0355	+0.0041
Dasgupta and Bhatia [56][a]	−1.2107	−0.5862	+0.8577	+0.1122
	−0.0230	−0.0169	+0.0359	+0.0046
Fon *et al.* [46]	−1.2228	−0.6323	+0.8730	+0.0941
	−0.0233[a]	−0.0158[a]	+0.0427[a]	+0.0034[a]
Present work; for details, see	−1.1986	−0.5916	+0.9508	+0.1090
Sauter and Meyer [76]	−0.0224	−0.0146	+0.0473	+0.0046
McEachran and Stauffer [64][b]	−1.2283	−0.6169	+0.9791	+0.1115
	−0.0233	−0.0171	+0.0395	+0.0044
Sienkiewicz and Baylis [59][a,c]	−1.2342	−0.6213	+1.0312	+0.1051
	−0.0230	−0.0171	+0.0438	+0.0044

[a]Interpolated values, using cubic polynomial fits to the nearest data points listed in the respective references.
[b]Listed phase shifts for $L \geqslant 1$ are weighted average of relativistic values—i.e., $\delta_L(L \geqslant 1)=[(L+1)\delta_{L+1/2}+L\delta_{L-1/2}]/(2L+1)$.
[c]Relativistic phase shifts for $L+1/2$.

range (5°–180°), using the Fribourg magnetic angle changer. In Fig. 4(b) the resulting DCS (open circles) is compared with the two sets of DCSs, calculated with the phase shifts of Fon *et al.* [46] and of SM [76]. The solid circles with error bars denote the results of independent experiments, yielding *absolute* values of the respective DCS. The open circles are (relative) DCS obtained with narrow angular spacing over limited angular ranges, using the detector at three fixed angular positions (45°, 90°, 135°) and magnetic angle scanning [48]. Remarkably good overall agreement of the experimental DCS with the two calculated DCSs is observed over the entire angular range. This suggests that the experimental DCS of [77] at the larger angles in Fig. 4(a) are too low.

Inspection of integral cross sections for electron-Ar scattering over the range 5–10 eV shows that the cross sections obtained with the phase shifts of SM [76] are in close overall agreement with the measured cross sections [65,71,77–81] while those of Fon *et al.* [46] are a bit lower and those of McEachran and Stauffer a bit higher.

In the analysis of the $Ar^-(3p^5 4s^2\ ^2P_{3/2,1/2})$ resonances, it became apparent that—in contrast to the situation for the $He^-(1s2s^2\ ^2S_{1/2})$ and the $Ne^-(2p^5 3s^2\ ^2P_{3/2,1/2})$ resonances—a satisfactory fit of the resonance profiles with energy-*independent* phase shifts was not possible. Thus energy-dependent phase shifts were extracted from the theoretical values by interpolation; the increments of the phase shifts from 11.00 eV to 11.36 eV are listed in Table I.

B. Scattering cross sections in the range of the $Ar^-(3p^5 4s^2\ ^2P_{3/2,1/2})$ resonances

A principal goal of the present work was an improved characterization of the low-lying, narrow Feshbach resonances $Ar^-(3p^5 4s^2\ ^2P_{3/2}, ^2P_{1/2})$. They correspond to bound states relative to the two metastable levels $Ar^*(3p^5 4s\ ^3P_2, ^3P_0)$, formed by spin-pairing another $4s$ electron to the respective metastable state. The corresponding binding energy is close to 0.45 eV [5], resulting in a rather extended $4s^2$ shell with a mean radius of about $9a_0$, which is of the same size as the wavelength of the incident electron of $7a_0$. Thus the resonances show up as sharp features in the scattering cross sections near 11.10 eV and 11.27 eV. We first present and analyze the Kaiserslautern data and subsequently the spectra measured in Fribourg.

As exploited and described previously in detail for He [22] and Ne [23], the absolute electron energy scale was calibrated with reference to the onset for production of the lowest metastable level. For argon, this is the $Ar^*(4s\ ^3P_2)$ level, located at 11.548 354(7) eV (see Sec. III A). In this way the energy of the incident electrons could be fixed to within 0.5 meV or better. Typically, the energy ranges 11.05–11.35 eV (resonance region) and 11.50–11.60 eV (onset for metastable atom production) were covered in each energy scan with energy intervals of 0.6 meV per channel. To correct for energy drifts, diagnosed from the apparent position of the $Ar^-(3p^5 4s^2\ ^2P_{3/2})$ resonance, five consecutive scans were summed (accumulation time 0.1 s per channel and scan), and the energy drifts between these summed scans were compensated by applying appropriate shifts on the respective relative energy scale (passive spectrum stabilization).

In Fig. 5 we present the result of 620 summed scans (accumulation time 62 s per channel) for the energy dependence of the elastic scattering signals at the five detection angles 22.5°, 45°, 90°, 112.5°, and 135°. The solid curves in Fig. 5 represent the results of *simultaneous* least-squares fits of theoretical cross sections to the data points, using the partial-wave formulas presented in Sec. II, the energy-dependent, nonresonant scattering phases for L=0–3 due to SM [76] and Fon *et al.* [46], and phases for the two resonances ac-

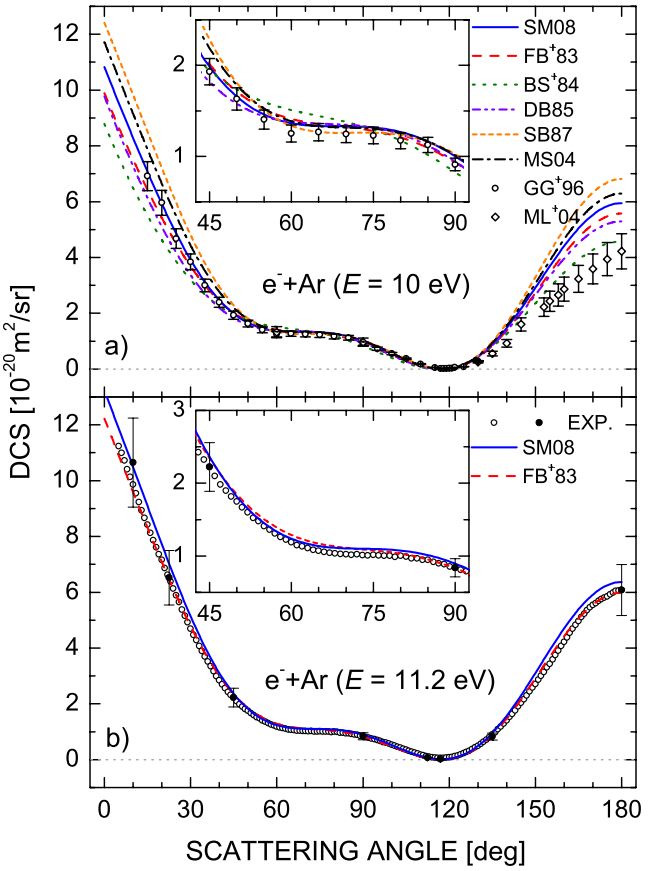

FIG. 4. (Color online) Absolute angle-differential cross sections for elastic electron-Ar scattering. (a) $E=10.0$ eV: The experimental cross sections of Gibson *et al.* [71] (GG$^+$96, open circles) and of Mielewska *et al.* [77] (ML$^+$04, open diamonds) are compared with the theoretical cross sections of Sienkiewicz and Baylis [59] (SB87), McEachran and Stauffer [64] (MS04), Fon *et al.* [46] (FB$^+$83), Sauter and Meyer (SM08, present work, see also [76]), Dasgupta and Bhatia [56] (DB85), and Bell *et al.* [55] (BS$^+$84). (b) $E=11.2$ eV: The results of the present experiment (Fribourg) are compared with the cross sections of Fon *et al.* [46] (FB$^+$83) and Sauter and Meyer [76] (SM08); the solid circles with error bars indicate the experimental absolute measurements at several discrete angles, the open circles result from magnetic scans with 1° increment, recorded at three fixed detector positions (45°, 90°, 135°) and normalized as described in Sec. III C and Ref. [48].

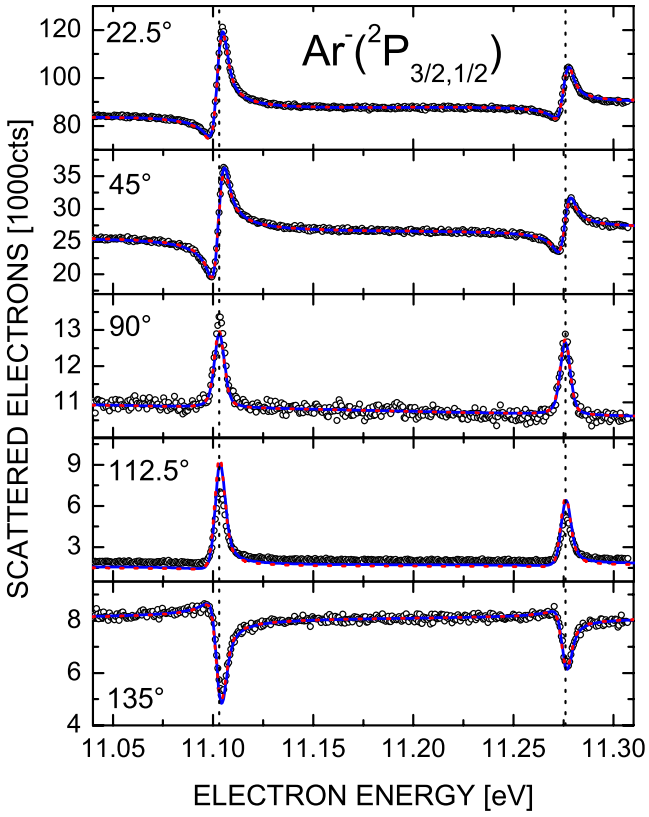

FIG. 5. (Color online) Profiles for the Ar$^-(3p^5 4s^2\ ^2P_{3/2,1/2})$ resonances, as simultaneously measured at the five scattering angles 22.5°, 45°, 90°, 112.5°, and 135° (open circles, respective average background of 9537, 904, 252, 323, 379 counts per channel subtracted). The blue solid and the red dashed curves show fitted resonance profiles which are calculated with the theoretical energy-dependent nonresonant phase shifts δ_L ($L=0-3$) due to Sauter and Meyer (present work and [76]) and Fon *et al.* [46], respectively, involving (consistently at the five angles) a Gaussian resolution function of width ΔE_{FWHM} and a single natural width Γ for both resonances. The fits yield $\Gamma=2.34$ meV and $\Gamma=2.25$ meV, respectively, $\Delta E_{\mathrm{FWHM}}=4.6$ meV in both cases, and a fine-structure separation of $\Delta_{\mathrm{FS}}=172.7$ meV.

cording to (4). The calculated cross sections were convoluted with a Gaussian function of adjustable width to simulate the overall energy resolution. In these analyses, the detector responses were fit parameters, thereby providing (partial) compensation of differences between the various angular-dependent nonresonant cross sections (see also the discussion below in connection with Fig. 6). In the fits of Fig. 5, possible weak signal contributions due to scattering from argon clusters, non-negligible at 112.5° (see Sec. III B 2), were ignored since the associated angular dependence is not known. The finite angular resolution (see Sec. III A) was neglected; test calculations showed a negligible influence of the angular acceptance range on the fitted resonance widths.

For most of the fit calculations we assumed that the two resonances have identical widths. Test calculations showed that the widths of the two resonances agree to within 5% with a tendency that the width of the $J=1/2$ resonance is about 0.1 meV *smaller* than the width of the $J=3/2$ resonance, in agreement with the prediction by Zatsarinny and Bartschat [26] and of present calculations (see below).

Analyses of the data in Fig. 5 were also carried out using other sets of nonresonant phase shifts (see Sec. IV A). In all cases, the fitted energy separation between the resonances was identical—namely, $\Delta_{\mathrm{FS}}=172.7$ meV—and we judge the uncertainty of this value to be at most 0.2 meV. The energy position of either resonance relative to the onset for production of metastable Ar*$(3p^5 4s\ ^3P_2)$ atoms varied by no more than 0.5 meV. The uncertainty in fixing the threshold for metastable atom production was typically 0.3 meV. The variation of the fitted resonance position with the choice of the nonresonant phase shifts amounted to no more than

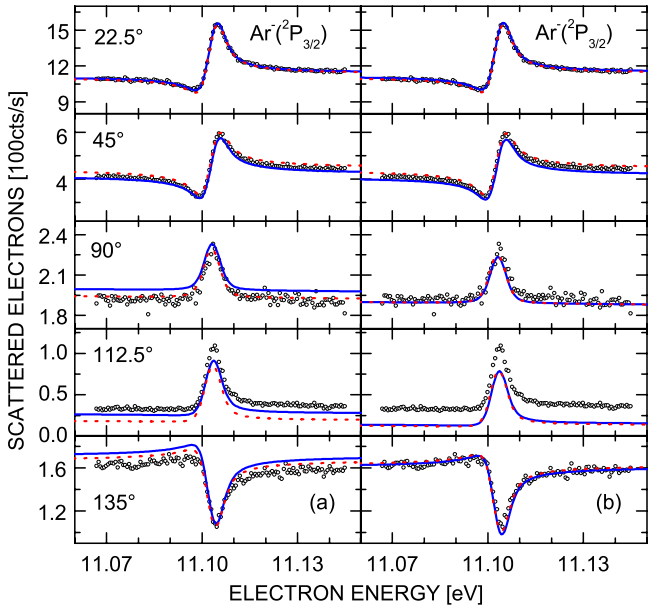

FIG. 6. (Color online) Profiles for the $Ar^-(3p^5 4s^2\ ^2P_{3/2})$ resonance (open circles), simultaneously measured at the indicated five scattering angles and corrected for the respective detector response, as calibrated against elastic scattering from He. The solid and dashed curves show fitted resonance profiles which are based on the nonresonant phase shifts δ_L (L=0–3) of Sauter and Meyer [76] and of Fon *et al.* [46], respectively. (a) The fits shown in the left panels involve a common (fitted) angle- and energy-independent background. (b) The fits shown in the right panels assume the absence of such a background at all angles.

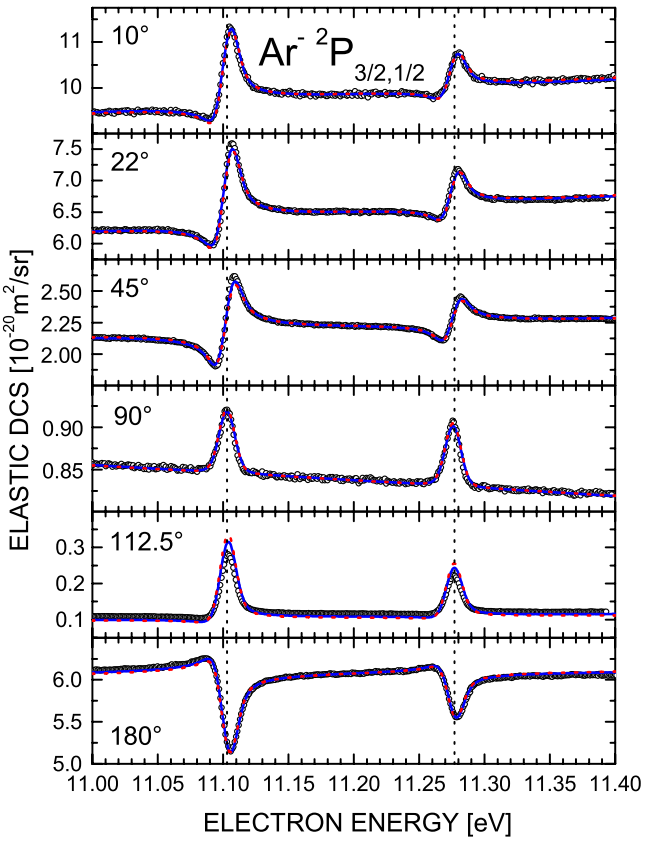

FIG. 7. (Color online) Profiles for the $Ar^-(3p^5 4s^2\ ^2P_{3/2,1/2})$ resonances, as measured with the Fribourg instrument with hemispherical analyzers. The spectra at 10° and 180° were measured with the magnetic angle changer. The blue solid and red dashed curves show fitted resonance profiles which are calculated with the theoretical energy-dependent nonresonant phase shifts δ_L (L=0–3) due to Sauter and Meyer [76] and Fon *et al.* [46], respectively.

0.5 meV. We conservatively quote the resonance energies with an overall error of 1 meV.

For the experimental data in Fig. 5 the fitted values of the resonance *width*, however, were found to vary significantly over the range 2.15–2.55 meV for the different choices of the nonresonant phase shifts. With the phases of Fon *et al.* [46] and SM [76], the fitted width amounted to 2.25 meV and 2.34 meV, respectively.

With the aim to provide spectra which were corrected for the detector response (which can vary with time), we carried out a sequence of measurements in which we scanned only the energy range of the $Ar^-(3p^5 4s^2\ ^2P_{3/2})$ resonance, but successively used He, Ar, and again He as target gases. In this way, the response factors R of the detectors (normalized to R=1 for the 22.5° detector) were fixed *in situ* for the relevant sampling time, yielding values of R=1.08, 1.27, 1.19, and 1.02 for the detectors at 45°, 90°, 112.5°, and 135°, respectively. Using these data, analyses of response-corrected spectra were performed *without* the freedom of adjustable response factors. In Fig. 6 we show these response-corrected data (open circles) and two fit results, based on the nonresonant phase shifts of SM [76] (blue solid curves) and of Fon *et al.* [46] (red dashed curves). Two different assumptions for signal contributions due to electron scattering from Ar clusters were made: (a) in the fits shown in the left panels we assume a common (fitted) angle- and energy-independent background; (b) in the fits shown in the right panels we assume that such a background is missing at all angles. In Fig. 6(b), fits of similar overall quality to the data—except for θ=112.5°—were obtained with fitted widths of 2.30 meV (ΔE=4.7 meV) and 2.26 meV (ΔE=4.8 meV), respectively. Assuming a common background [Fig. 6(a)] leads—except for θ=112.5°—to an overall reduction of the agreement between the experimental data and the fits with fitted widths of 2.37 meV (ΔE=4.7 meV) and 2.29 meV (ΔE=4.8 meV), respectively.

In view of the remaining uncertainties in the above analysis stemming from the possible background due to electron-scattering from Ar clusters it appeared opportune to verify the results using the Fribourg instrument with hemispherical analyzers, where the large nozzle (diameter 0.25 mm) and the low backing pressure (about 5 mbar) do not allow cluster formation and a larger angular range can be addressed. In Fig. 7 we compare the measured resonance profiles, normalized at E=11.2 eV to the experimental absolute DCS in Fig. 4(b) at each angle, with simultaneous fits of all the spectra using the phase shifts of SM [76] (blue solid curves) and Fon *et al.* [46] (red dashed curves). In these fits the absolute theoretical DCS was multiplied by a factor *close to unity*, fitted at *each* angle for optimal agreement with experiment for each set of phase shifts, thus compensating for small overall mismatches in the absolute theoretical and experi-

mental cross sections. Very good agreement is observed between the experimental and the fitted theoretical resonance profiles, yielding the resonance widths 2.33 meV (ΔE = 13.0 meV) and 2.23 meV (13.0 meV), respectively, and a fine-structure separation of 173.2 meV in both cases. Separate fits of the different spectra in Fig. 7 with the phase shifts of SM [76] yielded optimized values for the resonance width, the resolution, and the resonance spacing which were found to vary with angle θ as follows from 10° to 180° (θ:$\Gamma/\Delta E_{\mathrm{FWHM}}/\Delta_{\mathrm{FS}}$ in meV): 10°:2.22/12.6/173.4; 22.5°:2.26/11.8/172.3; 45°:2.29/11.6/172.9; 90°:2.06/11.4/173.0; 112.5°:1.30/12.5/172.8; 180°:2.43/13.9/173.2. The equally weighted average of these fitted resonance spacings amounts to 172.9 meV with an uncertainty of at most 0.6 meV; it is preferred over the value 173.2 meV obtained from the simultaneous fit which is dominated by the data with high signals.

We also carried out other fit calculations, again involving the three fit parameters Γ (identical for both resonances), ΔE, and Δ_{FS}, kept the same at all angles, but imposing less flexibility. (i) If the absolute theoretical DCSs are used without modification, substantial deviations between the measured and fitted theoretical spectra are obtained; they result from small differences between the absolute values of the experimental and the theoretical cross sections at energies away from the resonances. The resulting resonance widths came out unrealistically high or low. (ii) If the absolute theoretical DCS are multiplied by a *common* factor A for *all* angles (fitted for optimal agreement for each set of phase shifts, thus providing partial compensation for differences in the absolute theoretical and experimental cross sections), satisfactory fits to the experimental profiles were obtained, except for θ = 112.5° (and for 45° with the phase shifts of SM [76]). The fitted width came out as 2.26 meV (ΔE=12.9 meV, A = 1.02) with the phases of Fon *et al.* [46], whereas a rather small value of 2.10 meV (ΔE=12.0 meV, A=0.94) resulted with the phases of SM, apparently induced by the mismatch in the size of absolute cross sections at smaller angles. The deviations observed at 112.5° have little effect, since the DCS is small and thus has a low weight in the fitting procedure.

Our final result for the resonance width of the $^2P_{3/2}$ resonance is the weighted average of the various fits—namely, $\Gamma = (2.30 \pm 0.20)$ meV where the quoted error bar was chosen so wide that systematic uncertainties stemming from the nonresonant phase shifts and from the background due to electron scattering from Ar clusters are included in the error margin.

We note that the influence of the spin-orbit interaction on the continuum waves, resulting most notably in somewhat different phase shifts for the two p_j waves (j=3/2, 1/2), is small. Fits of the experimental spectra, using p_j phase shifts calculated by McEachran and Stauffer [64], did not significantly change the resonance width.

In Table II, we compare our experimental resonance width with those obtained in previous work. The widths, determined by Brunt *et al.* [82], Dubé *et al.* [24], and in the present work by a partial wave analysis of the resonance structure, agree within the mutual uncertainties. The widths derived by Hammond [25] from data measured at 112° with low statistical uncertainties and a quoted resolution of 12 meV have to be regarded as too large. It should be noted, however, that the widths reported in [25] were derived by fits using Fano-type line profiles (see, e.g., [83]) with adjustable widths and nonresonant background, and fixing the resolution at a value close to 12 meV. In a reanalysis of Hammond's data with his fitting procedure, we reproduced his resonance widths. If the resolution was raised to 15 meV, a resonance width of 2.4 meV was found with only slight degradation of the least-squares error. Fits of Hammond's spectrum based on the phase shifts of Fon *et al.* [46] or of SM [76] and assuming identical widths for the two resonances yielded widths of only 0.8 meV and 0.9 meV, respectively, at a fitted Gaussian resolution of 14.0 meV. These values are even lower than that of 1.3 meV, obtained from the Fribourg spectrum at 112.5°. We conclude from these observations that the ratio of the resonant to the nonresonant background cross section, calculated at angles around 112.5° with the phase shifts of Fon *et al.* [46] and SM [76], is not compatible with that measured by Hammond [25] and with the Fribourg instrument. Since in both these experiments "spurious" background is expected to be negligible, this incompatibility may indicate remaining deficiencies in the phase shifts underlying the analyses. Note that the size of the DCS near the deep minimum is the result of a destructive interference of the partial waves. Variations of the phase shifts showed, however, that improvements of the fits to the 112° resonance spectra (e.g., by raising the d-wave phase shift to values near 1.1 rad) are only possible at a significant loss of agreement between theory and experiment with regard to the overall angular dependence of the absolute DCS.

Theoretical widths are available from R-matrix calculations. The earlier widths of Ojha *et al.* [84] are too large by a factor of 2, while those of Scott *et al.* [85] are too small by

TABLE II. Widths Γ of the $Ar^-(3p^5 4s^2\ ^2P_{3/2,1/2})$ Feshbach resonances. In the second column, E represents experiment and T theory.

Author [reference]		Resonance width Γ (meV) $^2P_{3/2}$	$^2P_{1/2}$
Ehrhardt and co-workers [87,88]	E	<1	
Weingartshofer *et al.* [66]	E	3–4	
Brunt *et al.* [82]	E	2.5 ± 0.5	
Ojha *et al.* [84]	T	4.5	
Scott *et al.* [85]	T	1.58	1.70
Dubé *et al.* [24]	E	2.3 ± 0.2	
Hammond [25]	E	3.4 ± 0.2	3.2 ± 0.2
Zatsarinny and Bartschat [26]	T	2.2	2.1
Present theory (see also [76])	T	2.4 ± 0.4	
Present experiment	E	2.3 ± 0.2[a]	

[a]Fits of the experimental data shown in Fig. 5, allowing for nonidentical values of the widths for the $^2P_{3/2}$ and $^2P_{1/2}$ resonances, indicated that $\Gamma(^2P_{3/2}) \leqslant \Gamma(^2P_{1/2}) + 0.1$ meV.

TABLE III. Energies E_r and fine-structure (FS) splitting Δ_{FS} for the $Ar^-(3p^5 4s^2\ ^2P_{3/2,1/2})$ Feshbach resonances [here and in Table IV, the quoted uncertainties refer to the respective last digits—e.g., 172(2) means 172.7 ± 0.2]. In the second column, E represents experiment and T theory.

Author [reference]	E,T	Resonance energy E_r [eV]		FS splitting Δ_{FS} (meV)
		$^2P_{3/2}$	$^2P_{1/2}$	
Kuyatt *et al.* [89]	E	11.079(50)[a]	11.251(50)[a]	172(3)
Andrick and Ehrhardt [87]	E			173
Sanche and Schulz [90]	E	11.115(30)[a]	11.285(30)[a]	172(2)
Weingartshofer *et al.* [66]	E	11.125(10)[b]	11.297(10)[b]	172(5)
Brunt *et al.* [82]	E	11.098(10)	11.270(10)	172(1)
Ojha *et al.* [84]	T	11.127		
Scott *et al.* [85]	T	11.020	11.213	193
Hammond [25]	E	11.1030(3)	11.2763(3)	173.3
Zatsarinny and Bartschat [26]	T	11.098	11.270	172
Present experiment	E	11.1030(10)	11.2757(10)	172.7(2)

[a]Quoted values correspond to the center of the 30-meV-wide energy intervals given in the original papers, respectively.
[b]Quoted values were recalibrated, using the new value [19.365(1) eV [22]] for the energy of the $He^-(1s2s^2\ ^2S_{1/2})$ resonance.

30% and the energy dependence shows the opposite trend to what is indicated by our experiment. The width obtained in a recent *B*-spline *R*-matrix calculation [26] is in very good agreement with our recommended value, being located at our lower error limit. The calculated difference between the two widths of −0.1 meV is supported by our measurements. In the context of the present work, the resonance width has been investigated by applying Feshbach projection and Stieltjes imaging techniques, as described in an earlier application to the $He^-(1s2s^2)$ resonance [86]. The current result for the (average) width of 2.4(4) meV encloses the present recommended value. The relatively large uncertainty range reflects the ambiguities in the definition of the "continuum" and "resonance" subspaces, used in the Feshbach projection. The energy dependence of the width function, which is basically an exponential decrease with rising electron energy (as known from Penning ionization processes [86]), is relatively stable and results in a difference of −0.08(2) meV between the two resonances. More details will be given in [76].

In Table III, we compare the present values for the energy $E_{3/2}$ of the $Ar^-(3p^5 4s^2\ ^2P_{3/2})$ resonance and for the spin-orbit induced fine-structure splitting Δ_{FS} between the $^2P_{3/2}$ and $^2P_{1/2}$ resonances with earlier results. Both the resonance energies and the fine structure separations of Brunt *et al.* [82] (resolution about 19 meV) are found to agree with our more accurate values within the respective error limits. Excellent agreement is observed between our resonance energy $E_{3/2}$ and the previous benchmark result due to Hammond [25]. The fine-structure separation $\Delta_{FS}=173.3$ meV, inferred from the two resonance energies reported by Hammond, is slightly higher than our recommended value 172.7(2) meV; the Fribourg result 172.9(6) meV is in accordance with these two values.

C. Resonances in the excitation function for the production of metastable $Ar^*(4s\ ^3P_2, ^3P_0)$ atoms over the range 12.9–13.5 eV

The excitation function for the formation of metastable levels in the rare gas atoms is of interest for several applied plasmas such as discharges for lamps and gas lasers as well as for plasma etching. Until recently, theoretical results for these cross sections (see [91,92] and references therein) have shown substantial deviations from experimental data (see [5,27,28] and references therein). The recently introduced *B*-spline *R*-matrix (BSRM) theory [26,93] represents a major step forward, and very good agreement between the BSRM cross sections and the experimental cross sections has been observed for Ne [23,93] and Ar [26]. Here, we concentrate on the excitation function for the metastable $Ar(4s\ ^3P_{2,0})$ levels over the energy range 12.9–13.5 eV (see Fig. 8) in which prominent resonance structure due to anion levels associated with the neutral $Ar(3p^5 4p)$ configuration is observed (see Table II in [26]). The ten $Ar(3p^5 4p)$ levels are located between 12.9070 eV $(3p^5{}_{3/2}4p\ ^3S_1)$ and 13.4799 eV $(3p^5{}_{1/2}4p'\ ^1S_0)$ [41,42]. Within this energy range, BSRM theory predicted 11 resonances at the energy positions which are indicated by vertical dashed lines in Fig. 8 and labeled with numbers 13–23.

With respect to the resonance shapes, locations, and widths our experimental results are in excellent agreement with the BSRM results [26] with a single exception: at 13.152(1) eV we observe a peak with a width of 14 meV (addressed in Table IV as resonance 19*a*) whereas the calculations in [26] gave a flat peak structure at about 13.163 eV followed by a sharp window resonance of 1.6 meV width located at 13.168 eV (resonance number 19). We note that a later analysis [94] indicated that the sharp feature 19 is a numerical artifact. Our Fig. 7, therefore, was made with the

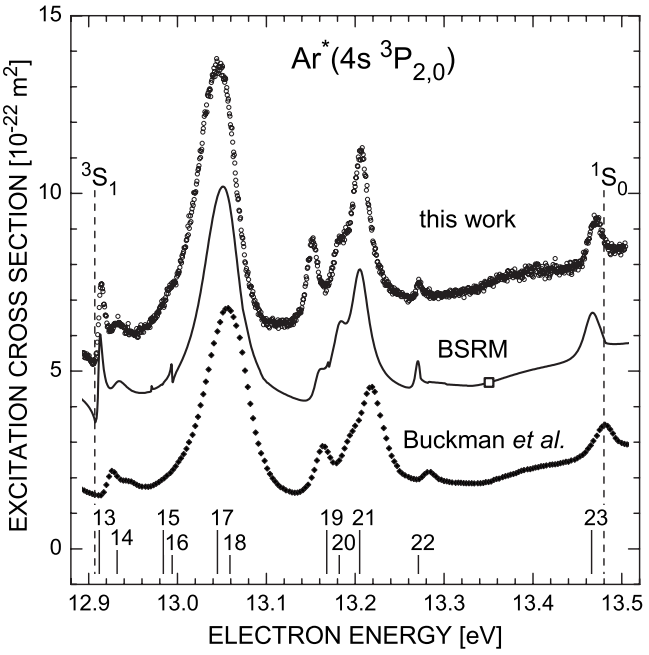

FIG. 8. Sum cross section for excitation of the two metastable $Ar(3p^5 4s\ ^3P_{2,0})$ levels (including cascade contributions at energies above 12.907 eV). Solid diamonds: experiment of Buckman *et al.* [28]; resolution 12–20 meV [95]. Solid curve: BSRM calculation [26,94]. Open circles: present experiment; resolution 5–6 meV (FWHM). The absolute cross-section scale refers to the theoretical data (normalization point at 13.35 eV). The relative experimental cross sections have been adjusted to the theoretical cross section at 13.35 eV and shifted by -2.8×10^{-22} m^2 (data of Buckman *et al.*) and $+2.8\times10^{-22}$ m^2 (this work) for clarity.

updated data file and slightly differs from the results published in [26]. Most importantly, however, the flat peak structure may need further theoretical reconsideration, using a more extended basis set. The features in the excitation spectrum of Buckman *et al.* [28] (see Fig. 7 and Table IV) are found to agree with our results, but they exhibit a general shift of 9 meV towards higher energies (which is within the quoted error bar of 10 meV for their energy calibration).

Due to the improved resolution in our experiment, some of the resonance structure is more pronounced than in the data of Brunt *et al.* [27] and in the later independent results of Buckman *et al.* [28], especially for the resonances 13, 14, and 22. The predicted sharp resonance 16 with a width of 1.4 meV and an energy of 12.994 eV is visible as a weak shoulder in our spectrum; it is remarkable that Buckman *et al.* [28] were able to locate a resonance feature at 12.99(1) eV, given their resolution of 12–20 meV [95].

D. Improved measurement of the $He^-(1s2s^2\ ^2S_{1/2})$ resonance

In connection with the test measurements involving the He target beam, we performed an improved study of the well-known $He^-(1s2s^2\ ^2S_{1/2})$ Feshbach resonance, located at $E_r=19.365(1)$ eV [22]. Compared to the data reported in [22] and in earlier work (see, e.g., [5,21,24], the new measurements (Fig. 9) have been carried out simultaneously at the five angles 22.5°, 45°, 90°, 112.5°, and 135° with an unprecedented effective resolution (6.2 meV FWHM) *and* good statistical quality.

Using the (energy-independent) nonresonant phase shifts due to Nesbet [40], as quoted in [22], simultaneous fit calculations of the five resonance profiles (solid curves in Fig. 9) were carried out; with the experimental and theoretical ordinate scales normalized at 22.5°, the fitted efficiencies for the detectors at 45°, 90°, 112.5°, and 135° (relative to the 22.5° detector) came out as 0.85, 0.90, 1.14, and 0.85, respectively. The overall analysis yielded the improved experimental value $\Gamma=10.9(3)$ meV for the resonance width and the experimental resolution 6.2(2) meV (FWHM). Within the mutual uncertainties this new value agrees very well with the

TABLE IV. Electron-argon scattering resonances in the vicinity of the $Ar(3p^5 4p)$ levels.

	Zatsarinny and Bartschat [26]			This work		Buckman *et al.* [5,28]	
No.	J^π	E (eV)	Γ (meV)	E (eV)	ΔE (meV)	E (eV)	ΔE (meV)
13	$3/2^-$	12.911[a]	5.9[b]	12.911(1)[a]	8(1)[b]	12.925(10)	
14	$1/2^-$	12.932	19.5	12.932(3)	20(3)	12.942(10)	
15	$5/2^-$	12.984	1.1				
16	$3/2^-$	12.994	1.4	12.994(4)		12.990(10)	
17	$1/2^-$	13.045	42.1	13.046(2)	52(3)	13.055(10)	52
18	$3/2^-$	13.059	39.3				
19	$1/2^-$	13.168	1.6				
19*a*				13.152(1)	14(1)	13.162(10)	23
20	$1/2^-$	13.182	19.3	13.182(2)[c]	17(3)[c]	13.190(10)	
21	$3/2^-$	13.205	24.7	13.206(1)	25(2)	13.216(8)	43
22	$1/2^+$	13.271	8.4	13.272(1)	8(1)	13.282(8)	27
23	$1/2^+$	13.466	25.5	13.471(1)	18(1)	13.479(8)	25

[a]Half-height position of the step.
[b]Min-max distance of the step.
[c]From "deconvolution."

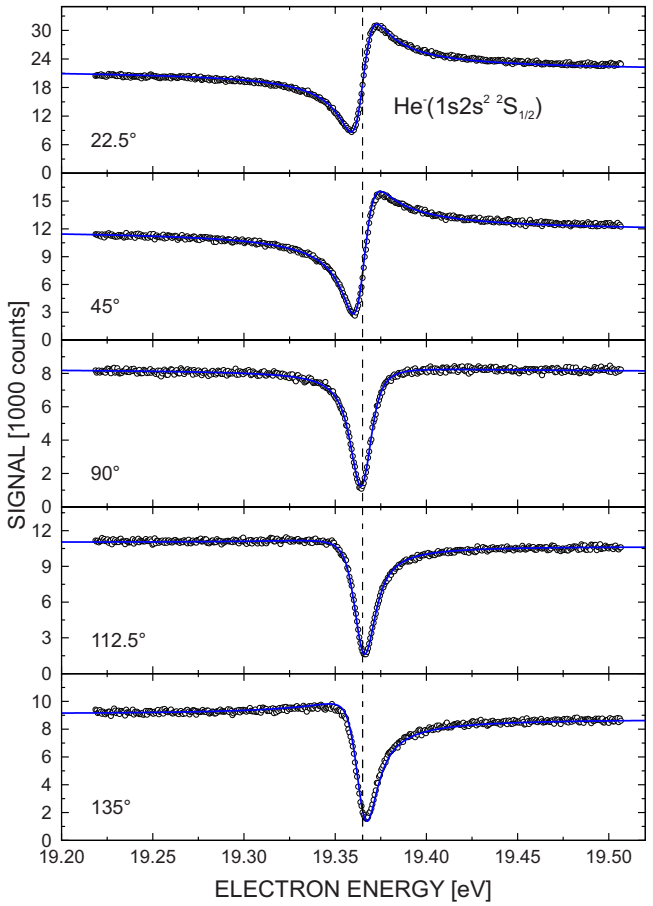

FIG. 9. (Color online) Profiles for the $He^-(1s2s^2\ ^2S_{1/2})$ Feshbach resonance, as simultaneously measured at five scattering angles from 22.5° to 135°. Open circles: experimental data (background subtracted). Solid curves: fitted resonance profiles involving (consistently at the five angles) a Gaussian resolution function with 6.2 meV full width at half maximum and a resonance width of $\Gamma = 10.9$ meV. The vertical dashed line indicates the resonance position $E_r = 19.365(1)$ eV [22].

experimental results obtained by Gopalan *et al.* (11.2(5) meV [22]), Kennerly *et al.* (11.0(5) meV [21]), and Allan and Franz (10.8(5) meV [96]), while the experimental value 10.3(3) meV, reported by Dubé *et al.* [24], is slightly lower. It is also in very good accordance with the recent theoretical results of Movre and Meyer (11.2 meV, Feshbach projection [86]) and of Gopalan *et al.* (10.7 meV, *R*-matrix [22]). For further comparisons with earlier work, see the discussion in [22,86].

V. CONCLUSIONS

Using two different experimental setups, we have reinvestigated elastic electron scattering from argon atoms in the energy range of the two low-lying $Ar^-(3p^5 4s^2\ ^2P_{3/2,1/2})$ Feshbach resonances at resolutions of about 5 meV and 13 meV, respectively. From detailed partial wave analyses of the experimental spectra, based on reliable theoretical nonresonant phase shifts (which were tested by comparing calculated and measured absolute angle-differential cross sections at 10 eV and 11.2 eV), we have determined accurate values for the natural widths [2.3(2) meV] and the fine-structure separation [172.7(2) meV] of the two resonances. From an *in situ* comparison of the energy onset for the production of metastable $Ar(3p^5 4s\ ^3P_2)$ atoms with the location of the Feshbach resonances, precise resonance energies were derived as 11.1030(10) eV ($^2P_{3/2}$) and 11.2757(10) eV ($^2P_{1/2}$). The energies and widths of some higher-lying resonances (12.9–13.5 eV), as studied in the excitation function for the formation of the two metastable $Ar(3p^5 4s\ ^3P_2, ^3P_0)$ levels at 5-meV resolution, have been determined and compared with the results of an earlier experiment [28] and of a recent *B*-spline *R*-matrix calculation [26]. From an improved measurement of the $He^-(1s2s^2\ ^2S_{1/2})$ resonance we have deduced a natural width of 10.9(3) meV.

ACKNOWLEDGMENTS

This work has been supported by the Deutsche Forschungsgemeinschaft through Forschergruppe FOR 307 as well as through Grant No. Ho 427/28, by the Forschungszentrum "Optische Technologien und Lasergesteuerte Prozesse," by the European Science Foundation through the network EIPAM ("Electron-Induced Processing At the Molecular level"), and by the Swiss National Science Foundation (Project No. 200020-113599). We gratefully acknowledge O. Zatsarinny, K. Bartschat, S. J. Buckman, P. Hammond, R. P. McEachran, A. D. Stauffer, and M. Zubek for helpful discussions or comments and for providing experimental or theoretical data in numerical form.

[1] G. J. Schulz, Rev. Mod. Phys. **45**, 378 (1973); **45**, 423 (1973).
[2] *Applied Atomic Collision Physics*, edited by H. S. W. Massey and D. R. Bates (Academic, New York, 1982), Vol. 1.
[3] *Electron-Molecule Collisions*, edited by I. Shimamura and K. Takayanagi (Plenum, New York, 1984).
[4] *Electron-Molecule Interactions and Their Applications*, edited by L. G. Christophorou (Academic, New York, 1984), Vols. 1 and 2.
[5] S. J. Buckman and C. W. Clark, Rev. Mod. Phys. **66**, 539 (1994).
[6] A. Zecca, G. P. Karwasz, and R. S. Brusa, Riv. Nuovo Cimento **19**, 1 (1995).
[7] L. G. Christophorou and J. K. Olthoff, Adv. At., Mol., Opt. Phys. **44**, 59 (2001); **44**, 155 (2001).
[8] M. J. Brunger and S. J. Buckman, Phys. Rep. **357**, 215 (2002).
[9] H. Hotop, M.-W. Ruf, M. Allan, and I. I. Fabrikant, Adv. At., Mol., Opt. Phys. **49**, 85 (2003).
[10] K. P. Rohr and F. Linder, J. Phys. B **9**, 2521 (1976).
[11] K. Jung, Th. Antoni, R. Müller, K. H. Kochem, and H. Ehrhardt, J. Phys. B **15**, 3535 (1982).

[12] F. H. Read, Phys. Scr. **27**, 103 (1983).
[13] M. Allan, J. Phys. B **28**, 5163 (1995).
[14] M. Allan, Phys. Rev. Lett. **87**, 033201 (2001).
[15] A. Chutjian, A. Garscadden, and J. M. Wadehra, Phys. Rep. **264**, 393 (1996).
[16] D. Field, G. Mrotzek, D. W. Knight, S. Lunt, and J. P. Ziesel, J. Phys. B **21**, 171 (1988).
[17] D. Field, D. W. Knight, G. Mrotzek, J. Randell, S. L. Lunt, J. B. Ozenne, and J. P. Ziesel, Meas. Sci. Technol. **2**, 757 (1991).
[18] D. Field, S. L. Lunt, and J. P. Ziesel, Acc. Chem. Res. **34**, 291 (2001).
[19] S. V. Hoffmann, S. L. Lunt, N. C. Jones, D. Field, and J.-P. Ziesel, Rev. Sci. Instrum. **73**, 4157 (2002).
[20] R. J. van Brunt and A. C. Gallagher, in *Electronic and Atomic Collisions*, edited by G. Watel (North-Holland, Amsterdam, 1978), p. 129f.
[21] R. E. Kennerly, R. J. Van Brunt, and A. C. Gallagher, Phys. Rev. A **23**, 2430 (1981).
[22] A. Gopalan, J. Bömmels, S. Götte, A. Landwehr, K. Franz, M.-W. Ruf, H. Hotop, and K. Bartschat, Eur. Phys. J. D **22**, 17 (2003).
[23] J. Bömmels, K. Franz, T. H. Hoffmann, A. Gopalan, O. Zatsarinny, K. Bartschat, M.-W. Ruf, and H. Hotop, Phys. Rev. A **71**, 012704 (2005).
[24] D. Dubé, D. Tremblay, and D. Roy, Phys. Rev. A **47**, 2893 (1993).
[25] P. Hammond, J. Phys. B **29**, L231 (1996).
[26] O. Zatsarinny and K. Bartschat, J. Phys. B **37**, 4693 (2004).
[27] J. N. H. Brunt, G. C. King, and F. H. Read, J. Phys. B **9**, 2195 (1976).
[28] S. J. Buckman, P. Hammond, G. C. King, and F. H. Read, J. Phys. B **16**, 4219 (1983).
[29] N. F. Mott and H. S. W. Massey, *The theory of Atomic Collisions* (Oxford University Press, Oxford, 1965).
[30] D. G. Thompson, J. Phys. B **4**, 468 (1971).
[31] D. Andrick, Adv. At. Mol. Phys. **9**, 271 (1973).
[32] T. M. Miller and B. Bederson, Adv. At. Mol. Phys. **13**, 1 (1978).
[33] D. G. Thompson, Proc. R. Soc. London, Ser. A **294**, 160 (1966).
[34] S. Götte, A. Gopalan, J. Bömmels, M.-W. Ruf, and H. Hotop, Rev. Sci. Instrum. **71**, 4070, (2000).
[35] R. Campargue, J. Phys. Chem. **88**, 4466 (1984).
[36] J. M. Weber, M.-W. Ruf, and H. Hotop, Eur. Phys. J. D **7**, 587 (1999).
[37] I. D. Petrov, V. L. Sukhorukov, E. Leber, and H. Hotop, Eur. Phys. J. D **10**, 53 (2000).
[38] J. Bömmels, E. Leber, A. Gopalan, J.-M. Weber, S. Barsotti, M.-W. Ruf, and H. Hotop, Rev. Sci. Instrum. **72**, 4098 (2001).
[39] A. Gopalan, E. Leber, J. Bömmels, S. P. H. Paul, M. Allegrini, M.-W. Ruf, and H. Hotop, Eur. Phys. J. D **30**, 163 (2004).
[40] R. K. Nesbet, Phys. Rev. A **20**, 58 (1979).
[41] L. Minnhagen, J. Opt. Soc. Am. **63**, 1185 (1973).
[42] I. Velchev, W. Hogervorst, and W. Ubachs, J. Phys. B **32**, L511 (1999).
[43] P. J. Mohr and B. N. Taylor, Rev. Mod. Phys. **77**, 1 (2005).
[44] D. Klar, M.-W. Ruf, and H. Hotop, Aust. J. Phys. **45**, 263 (1992).
[45] A. Schramm, J. M. Weber, J. Kreil, D. Klar, M.-W. Ruf, and H. Hotop, Phys. Rev. Lett. **81**, 778 (1998).
[46] W. C. Fon, K. A. Berrington, P. G. Burke, and A. Hibbert, J. Phys. B **16**, 307 (1983).
[47] F. H. Read and J. M. Channing, Rev. Sci. Instrum. **67**, 2372 (1996).
[48] M. Allan, J. Phys. B **38**, 3655 (2005).
[49] E. A. Garbaty and R. W. LaBahn, Phys. Rev. A **4**, 1425 (1971).
[50] M. S. Pindzola and H. P. Kelly, Phys. Rev. A **9**, 323 (1974).
[51] A. W. Yau, R. P. McEachran, and A. D. Stauffer, J. Phys. B **13**, 377 (1980).
[52] M. Y. Amusia, N. A. Cherepkov, L. V. Chernysheva, D. M. Davidovic, and V. Radojevic, Phys. Rev. A **25**, 219 (1982).
[53] R. P. McEachran and A. D. Stauffer, J. Phys. B **16**, 4023 (1983).
[54] J. K. O'Connell and N. F. Lane, Phys. Rev. A **27**, 1893 (1983).
[55] K. L. Bell, N. S. Scott, and M. A. Lennon, J. Phys. B **17**, 4757 (1984).
[56] A. Dasgupta and A. K. Bhatia, Phys. Rev. A **32**, 3335 (1985).
[57] H. Nakanishi and D. M. Schrader, Phys. Rev. A **34**, 1823 (1986).
[58] S. N. Nahar and J. M. Wadehra, Phys. Rev. A **35**, 2051 (1987).
[59] J. E. Sienkiewicz and W. E. Baylis, J. Phys. B **20**, L627 (1987).
[60] B. Plenkiewicz, P. Plenkiewicz, and J.-P. Jay-Gerin, Phys. Rev. A **38**, 4460 (1988).
[61] H. P. Saha, Phys. Rev. A **43**, 4712 (1991); see also the results cited in [71].
[62] D. J. R. Mimnagh, R. P. McEachran, and A. D. Stauffer, J. Phys. B **26**, 1727 (1993).
[63] C. Kerner and W. Meyer (unpublished); C. Kerner, Ph. D. dissertation, University of Kaiserslautern, 1995 (unpublished).
[64] R. P. McEachran and A. D. Stauffer, Aust. J. Phys. **50**, 511 (1997); and (private communication).
[65] A. Bitsch, Diplomarbeit, University of Kaiserslautern, 1972 (unpublished); also cited in the literature as D. Andrick and A. Bitsch or D. Andrick (private communication) or (unpublished) (1973 or 1983 or 1984).
[66] A. Weingartshofer, K. Willmann, and E. M. Clarke, J. Phys. B **7**, 79 (1974).
[67] J. F. Williams and B. A. Willis, J. Phys. B **8**, 1670 (1975).
[68] J. F. Williams, J. Phys. B **12**, 265 (1979).
[69] S. K. Srivastava, H. Tanaka, A. Chutjian, and S. Trajmar, Phys. Rev. A **23**, 2156 (1981).
[70] J. E. Furst, D. E. Golden, M. Mahgerefteh, J. Zhou, and D. Mueller, Phys. Rev. A **40**, 5592 (1989).
[71] J. C. Gibson, R. J. Gulley, J. P. Sullivan, S. J. Buckman, V. Chan, and P. D. Burrow, J. Phys. B **29**, 3177 (1996).
[72] K. Franz, Ph.D. dissertation, Technische Universität Kaiserslautern, 2005 (unpublished).
[73] R. D. Cowan, *Theory of Atomic Structure and Spectra* (University of California Press, Berkeley, 1981).
[74] R. P. McEachran and A. D. Stauffer, J. Phys. B **23**, 4605 (1990).
[75] D. Spelsberg and W. Meyer, *Abstracts of Contributed Papers, 23rd International Conference on Photonic, Electronic, and Atomic Collisions*, edited by J. Anton, H. Cederquist, M. Larsson, E. Lindroth, S. Mannervik, H. Schmidt, and R. Schuch (Stockholm University, Stockholm, Sweden, 2003), Vol. II, p. Tu057.
[76] G. Sauter and W. Meyer (unpublished).

[77] B. Mielewska, I. Linert, G. C. King, and M. Zubek, Phys. Rev. A **69**, 062716 (2004).
[78] J. C. Nickel, K. Imre, D. F. Register, and S. Trajmar, J. Phys. B **18**, 125 (1985).
[79] J. Ferch, B. Granitza, C. Masche, and W. Raith, J. Phys. B **18**, 967 (1985).
[80] C. Szmytkowski, K. Maciag, and G. Karwacz, Phys. Scr. **54**, 271 (1996).
[81] W. Y. Baek and B. Grosswendt, J. Phys. B **36**, 731 (2003).
[82] J. N. H. Brunt, G. C. King, and F. H. Read, J. Phys. B **10**, 1289 (1977).
[83] U. Fano and J. W. Cooper, Phys. Rev. **137**, A1364 (1965).
[84] P. Ojha, P. G. Burke, and K. T. Taylor, J. Phys. B **15**, L507 (1982).
[85] N. S. Scott, K. L. Bell, P. G. Burke, and K. T. Taylor, J. Phys. B **15**, L627 (1982).
[86] M. Movre and W. Meyer, J. Chem. Phys. **106**, 7139 (1997).
[87] D. Andrick and H. Ehrhardt, Z. Phys. **192**, 99 (1966).
[88] H. Ehrhardt, L. Langhans, F. Linder, and H. S. Taylor, Phys. Rev. **173**, 222 (1968).
[89] C. E. Kuyatt, J. A. R. Simpson, and S. R. Mielczarek, Phys. Rev. **138**, A385 (1965).
[90] L. Sanche and G. J. Schulz, Phys. Rev. A **5**, 1672 (1972).
[91] D. H. Madison, C. M. Maloney, and J. B. Wang, J. Phys. B **31**, 873 (1998).
[92] A. N. Grum-Grzhimailo and K. Bartschat, J. Phys. B **34**, L727 (2001).
[93] O. Zatsarinny and K. Bartschat, J. Phys. B **37**, 2173 (2004).
[94] O. Zatsarinny and K. Barschat (private communication).
[95] S. J. Buckman (private communication).
[96] M. Allan and K. Franz (unpublished).